63-4-1

WATKINS-JOHNSON COMPANY
electron devices
electronic systems

Interim Engineering Report No. 8

APPLIED RESEARCH ON A HIGH-POWER MILLIMETER-WAVE GENERATOR

By
M. V. Purnell

Watkins-Johnson Company
3333 Hillview Avenue
Palo Alto, California

1 March 1963 through 31 May 1963

Contract No. AF 33(616)-8369
Task No. 415603

The applied research reported in this document has been made possible through support and sponsorship extended by the Electronic Technology Laboratory of the Aeronuatical Systems Division, under Contract AF 33(616)-8369. It is published for technical information only and does not necessarily represent recommendations or conclusions of the sponsoring agency.

ABSTRACT

The purpose of this program is to demonstrate the feasibility of generating very high power, specifically 100 kw peak and 1000 watt average at 100 Gc by means of an O-type backward-wave oscillator operating at very high voltage.

During the eighth quarter, experimental tube No. 3 was completed and some test data has been obtained. Testing of tube No. 3 will be continued during the next quarter of the program. Peak and average power have been measured at 107 kw and 215 watts respectively. Very recent results have shown average power of over 300 watts.

The 435-1C gun is used in tube No. 3. Test results show improved focusing with a reduced magnetic field as compared with guns used in previous tubes.

The rf output power is terminated in helical stainless steel waveguides. These rf loads are water cooled for use with the calorimeter for average power measurement. A tungsten insert was used to collimate the electron beam at the anode to prevent peak heating damage to the disk loaded waveguide circuit.

TABLE OF CONTENTS

	Page No.
INTRODUCTION	1
TUBE CONSTRUCTION	1
Electron Gun and Circuit	1
Tungsten Insert and Circuit	5
Helical Waveguide Loads	5
Load Calibrations	5
Construction of Tube No. 4	11
TUBE NO. 3 TESTING	11
435-1C Gun	11
Measurement of Frequency	14
Average Power	14
Peak Power Measurements	14
Pulse Shapes	18
Beam Voltage	18
Higher Order Oscillation	18
REFERENCES	32
APPENDIX I	33
APPENDIX II	34

LIST OF ILLUSTRATIONS

		Page No.
Fig. 1	Photograph of tube No. 3 during vacuum processing.	2
Fig. 2	Geometry of 435-1C gun.	2
Fig. 3	Predicted beam diameter vs beam voltage for guns No. 9, 435-1B and 435-1C.	4
Fig. 4	The disk loaded waveguide circuit is shown with collector and anode pole pieces.	6
Fig. 5	Anode-cathode assembly of gun 435-1C as it is being used in tube No. 3.	7
Fig. 6	The helical waveguide loads used on tube No. 3.	8
Fig. 7	Helical attenuator calibration used on tube No. 3.	9
Fig. 8	Variable attenuator calibration used on tube No. 3.	10
Fig. 9	Beam transmission is plotted vs beam voltage on tube No. 3.	11
Fig. 10	Tube No. 3 beam current vs beam voltage plotted on 2/3 power graph paper.	12
Fig. 11	Magnet field required to focus each of the three tubes built.	13
Fig. 12	Frequency measured using a wavemeter vs beam voltage on tubes No. 1 and 2.	15
Fig. 13	Block diagram of calorimeter measurement of average power.	16
Fig. 14	RF pulse viewed using a crystal detector compaired with equivalent rectangular pulse.	19

List of Illustrations (continued) Page No.

Fig. 15	The graph shows the peak output power vs beam voltage.	20
Fig. 16	Collector and body current at 126 kv beam voltage.	21
Fig. 17	Collector and body current at 144 kv beam voltage.	22
Fig. 18	Collector and body current at 162 kv beam voltage.	23
Fig. 19	Collector and body current at 180 kv beam voltage.	24
Fig. 20	Collector and body current at 193 kv beam voltage.	25
Fig. 21	Cathode voltage pulse and detected rf pulse at 126 kv.	26
Fig. 22	Cathode voltage pulse and detected rf pulse at 144 kv.	27
Fig. 23	Cathode voltage pulse and detected rf pulse at 162 kv.	28
Fig. 24	Cathode voltage pulse and detected rf pulse at 180 kv.	29
Fig. 25	Cathode voltage pulse and detected rf pulse at 193 kv.	30

LIST OF TABLES

		Page No.
Table I	The peak power was calculated based on the average power measured, using the calorimeter.	17
Table II	Table II contains a list of the pulse shapes shown in Figs. 16 through 25.	31

INTRODUCTION

The purpose of this program is to demonstrate the feasibility of generating very high power, specifically 100 kw peak and 1000 watts average at 100 Gc by means of an O-type backward-wave oscillator operating at very high voltage.

During the eighth quarter, tube No. 3 was completed and some data has been measured. The 435-1C gun was used in this tube which resulted in 96 percent transmission with a considerable reduction in magnetic field over that necessary in tubes No. 1 and 2. Peak and average power have been measured as 107 kw and 215 watts respectively. This is a fraction of four times greater than the previous 47 watts measured on tube No. 1. This represents a new record for average power at this frequency.

Construction of tube No. 4 has been started. The collector assembly is completed. The circuit assembly is complete except for connection of pole pieces. The gun assembly has been started and will use the 435-1C gun that is in tube No. 3. Target date for completion of tube No. 4 is 1 July 1963. During the writing of this report even higher average power of over 300 watts were observed.

TUBE CONSTRUCTION

Tube No. 3 was completed and testing is now in progress. It was necessary to reprocess tube No. 3 because of a bad cathode. The gun was removed and rebuilt. The tube was then reprocessed on the vacuum pump. Tube No. 3 is shown in Fig. 1.

Electron Gun and Circuit

The 435-1C electron gun was used in tube No. 3. The electrical geometry of this gun is shown in Fig. 2. This gun has a predicted beam diameter vs beam voltage as shown in Fig. 3. Beam size is compared with the tube No. 9 and 435-1B guns used in tubes No. 1 and 2 respectively. The transmission and perveance data are given in Figs. 9 and 10 as

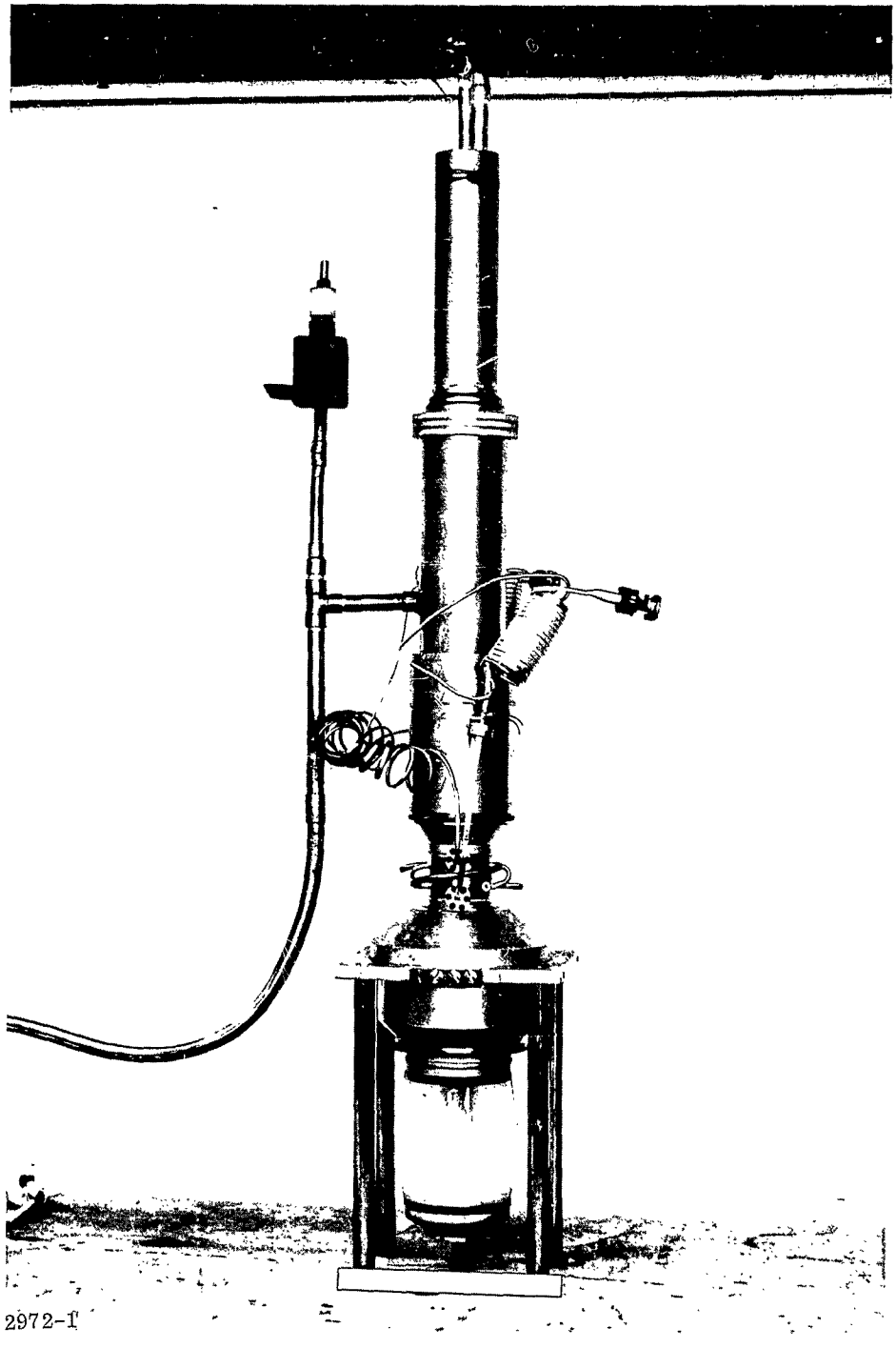

Fig. 1 - Tube No. 3 is shown during vacuum processing. Average power is measured using a calorimeter on the two tight wound helical waveguide loads. The loose wound helical waveguide terminates the collector end of the disk loaded waveguide circuit. An average power of 215 watts was measured with loads and waveguide as shown. It is planned to water cool the waveguides between the circuit and helical loads before higher average power measurements are attempted.

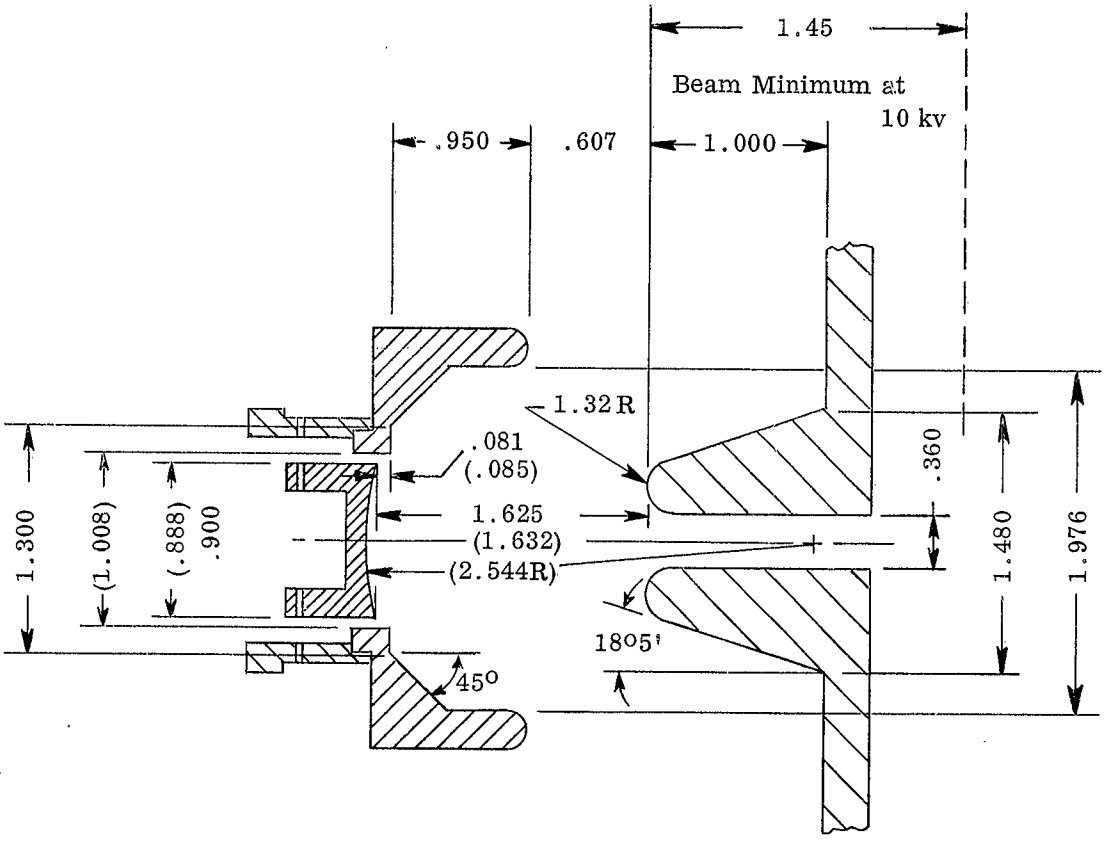

Dimensions in brackets
cold, all others hot

Fig. 2 - Gun 435-1C dimensions as tested in demountable beam analyzer. Gun 435-1C is identical to gun 435-1B with the exception that the cathode is recessed deeper into the focus electrode. This gun is used in tube No. 3.

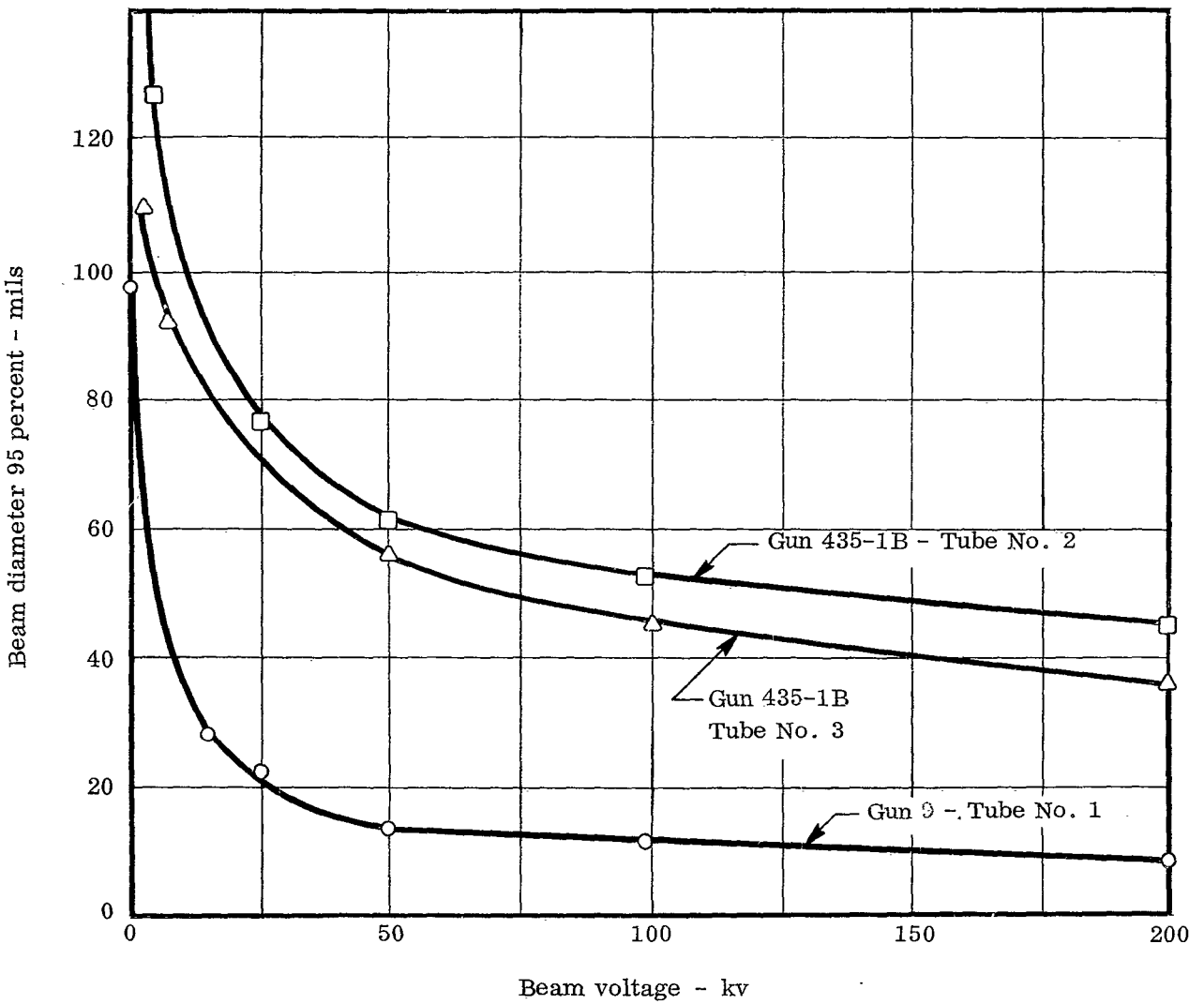

Fig. 3 - Diameter enclosing 95 percent of the beam current plotted as a function of beam voltage for gun No. 9 which was used in tube No. 1, for gun 435-1B which is being used in tube No. 2 and for gun 435-1C used in tube No. 3. These curves were obtained from the results of Danielson, Rosenfeld, and Saloom[1] as generalized by Herrmann[2].

measured during the tests on tube No. 3.

Tungsten Insert and Circuit

The electron formed disk loaded waveguide circuit with anode and collector pole process is shown in Fig. 4. The anode pole piece contains a tungsten insert with a .062 inch diameter hole to collimate the electron beam and prevent peak heating damage to the .070 inch diameter circuit. Tungsten was used as an insert because of its high melting point and its low vapor pressure with high temperature. Appendix I shows copper to be 1.8 times better than tungsten relative to temperature rise, but the melting point of tungsten is 3370°C compared with 1080°C for copper. Test results, to date, on tube No. 3 indicate no damage due to peak heating after operating up to voltages of 198 kv. Figure 5 shows the tungsten insert in the anode-cathode assembly of tube No. 3.

Helical Waveguide Loads

In tube No. 3 a helical-waveguide attenuator is used between the disk loaded waveguide circuit of the tube and the rf vacuum window. These loads are formed by rolling a length of round thin walled stainless steel tubing into rectangular .050" x .100" waveguide. This rectangular waveguide load is then formed into a tight wound helix. A cylinder of copper is brazed inside the helical load and a coil of copper tubing is brazed inside the copper cylinder for water cooling and for use with the calorimeter. Figure 6 shows the helical waveguide load used on tube No. 3. Two of these loads are used to terminate the two outputs of the tube. A single coil of stainless steel waveguide is connected between the two connectors at the collector end of the disk loaded waveguide circuit as a termination. These helical waveguide loads can be seen on tube No. 3 (shown in Fig. 1). Each of the helical waveguides used on tube No. 3 is 6 ft. long and have about 27 db of attenuation. Peak power at the rf vacuum window is about 100 watts.

Load Calibrations

The 100 watts external to the vacuum is further attenuated by use of the same type stainless steel helical attenuator used for the calorimeter loads and by a variable attenuator. Peak power can be viewed using a crystal operating at the 1 mw level. Calibration results for the attenuator used as vacuum loads and external to the vacuum are shown in Fig. 7. The attenuation calibration is based on relative power levels using a crystal and a VSWR meter. Accuracy of ± 2 db is about the best to be expected from this method of calibration. The variable attenuator was also calibrated by use of a crystal and VSWR meter. Figure 8 shows the calibration results for the variable attenuator used in the rf detector circuit. The crystal could not be calibrated to some absolute power level due to the lack of a directed reading calorimeter at these frequencies. The crystal was calibrated on the basis of its

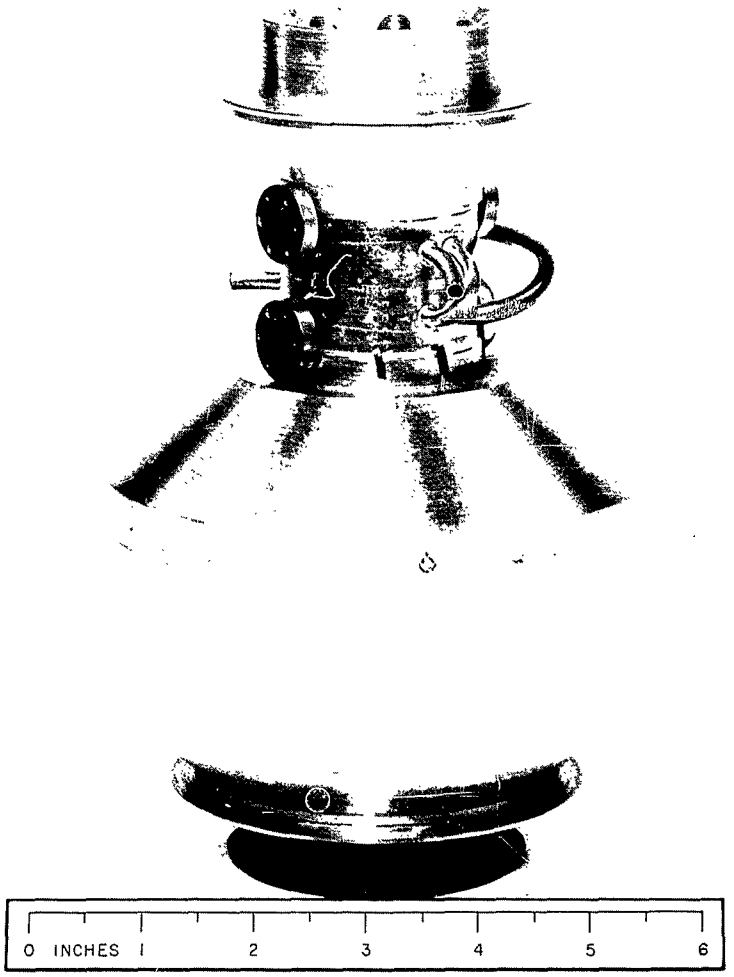

WATKINS JOHNSON

2963

Fig. 4 - The disk loaded waveguide circuit is shown with collector and anode pole pieces. The circuit is water cooled using the copper tubing shown. Power is removed from the circuit at the gun end using .050 x .100 inch copper waveguide to connect with the stainless steel helical waveguide loads. The collector end of the circuit is terminated in a single helical waveguide (see Fig. 1).

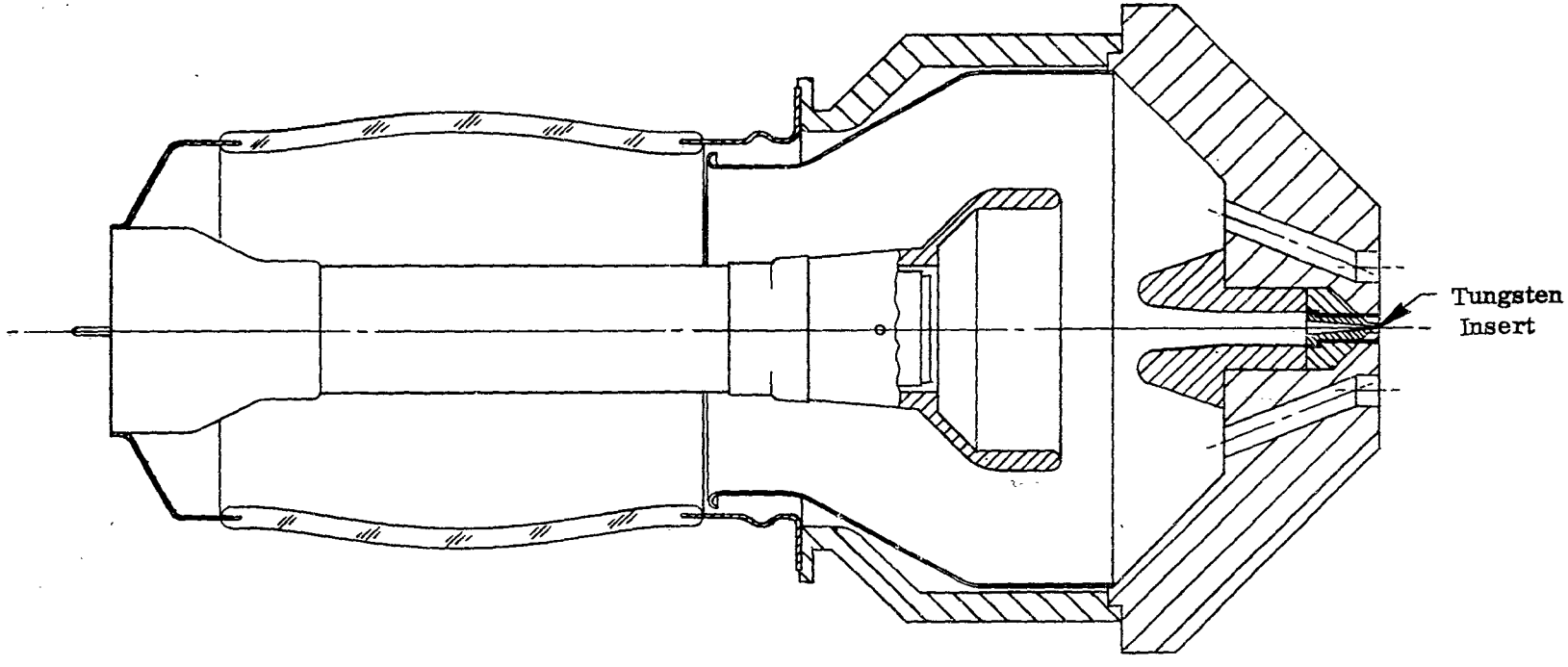

Fig. 5 - Anode-cathode assembly of gun 435-1C as it is being used in tube No. 3. The tungsten insert was placed in the anode pole piece to collimate the beam to prevent peak heating damage to the disk loaded waveguide circuit when operating at high voltage. The hole size in the tungsten insert is .062 inch, compared with .070 inch circuit diameter of the disk loaded waveguide circuit.

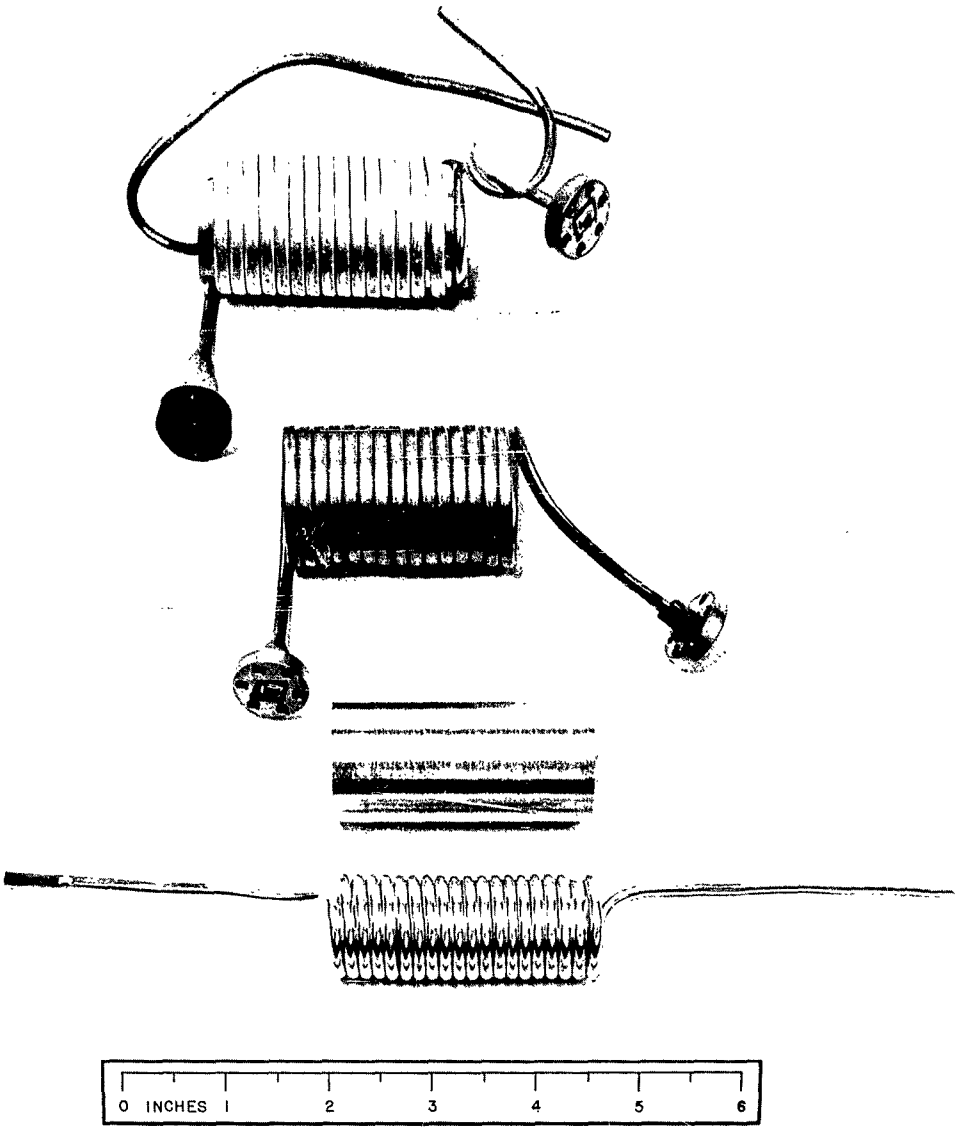

Fig. 6 - The helical waveguide load is shown as the top assembly in the figure. The three elements that make up the assembly are shown below. Two each of these loads are used per tube since the match to the circuit splits the power equally between output.

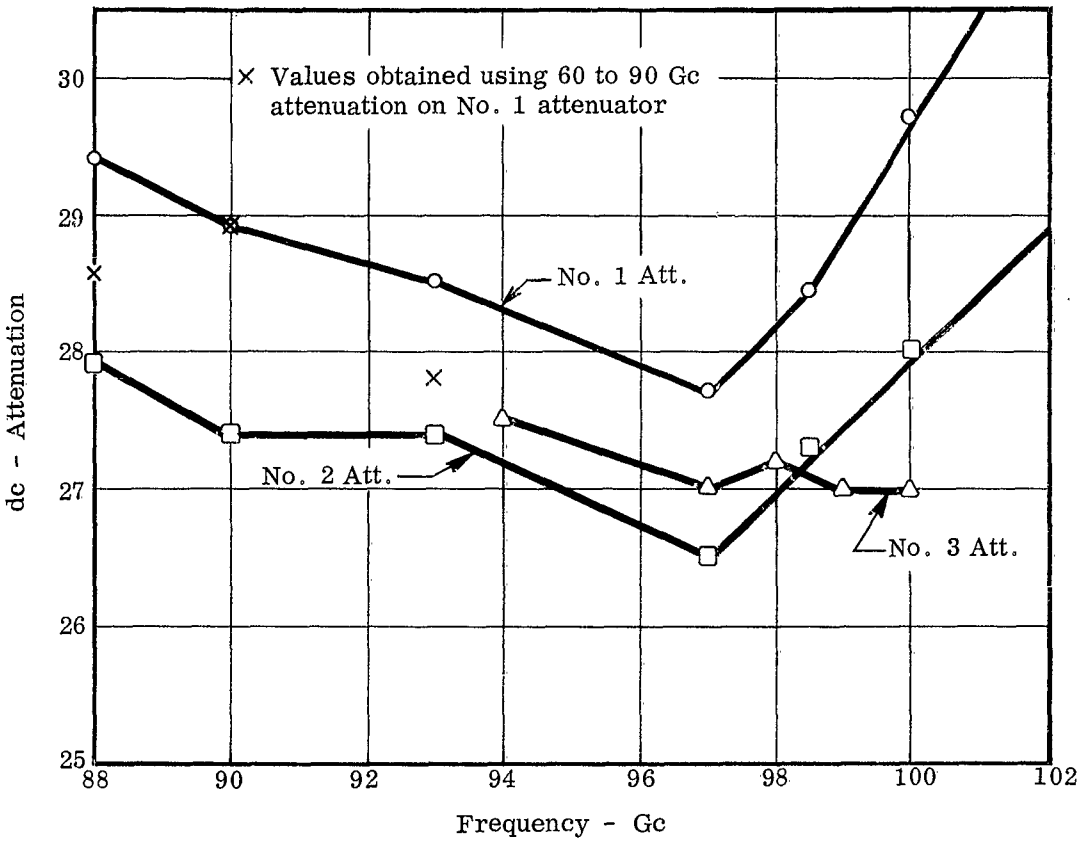

Fig. 7 - The attenuators were calibrated using a crystal and VSWR meter. The relative power levels were measured at the input and output of the helical waveguide attenuators. The attenuation was based on this difference of power levels. A 60 to 90 Gc precision attenuator was used to check the values measured below 93 Gc. The result using the precision attenuator are shown on the above curve for attenuator No. 1. These points are shown by x. Data above 93 Gc was all based on the use of the crystal and VSWR meter.

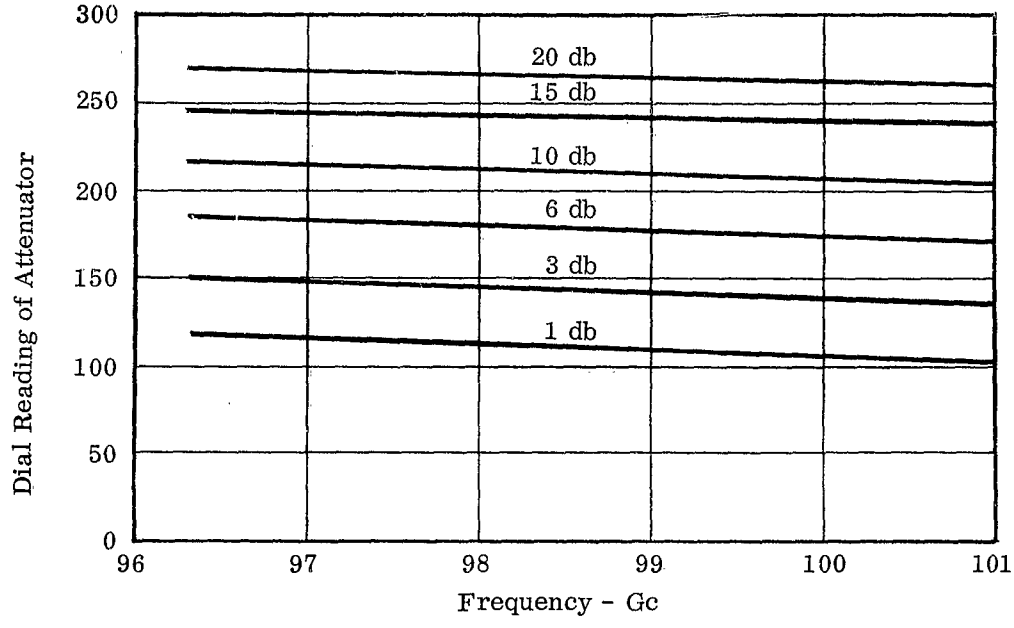

Fig. 8 - The attenuation of the variable attenuator used to vary detected output pulse. The above data is based on calibration using a crystal detector and measuring level changes on a VSWR meter.

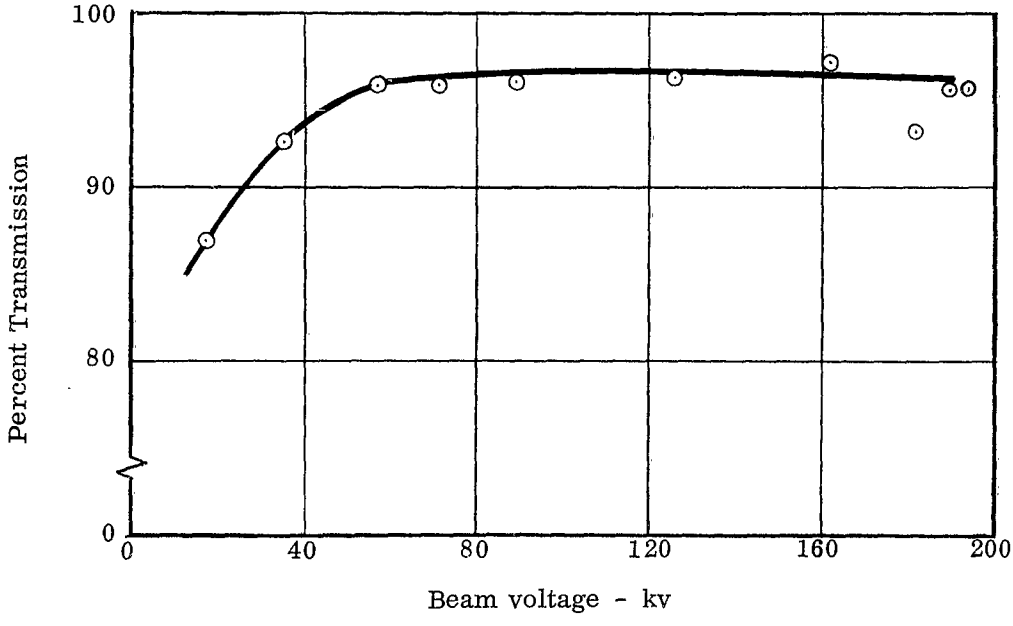

Fig. 9 - Beam transmission is plotted vs beam voltage on tube No. 3. This tube uses the 435-1C electron gun which results in good transmission with reduced magnetic field compared with electron guns used in tubes No. 1 and 2.

11743

level reading on a VSWR meter as compared with readings obtained with calibrated crystal at other frequency bands. This calibration did produce results that agree with the values measured using the average power to calculate peak power. See Fig. 15. Since tube No. 3 can produce large average power which can be measured on a calorimeter, the use of the above attenuator calibrations is not necessary for the measurement of peak power. Best peak power measurements is based on average power and duty cycle.

Construction of Tube No. 4

Tube No. 4 will be built the same as tube No. 3. This tube should be completed by 1 July 1963. Most of the assemblies are complete except for the 435-1C gun and the helical waveguide loads.

TUBE NO. 3 TESTING

435-1C Gun

The 435-1C gun is used on tube No. 3 (see Fig. 2). The 435-1C has a predicted beam diameter shown by Fig. 3. The beam transmission of tube No. 3 is shown in Fig. 9. For voltages less than 60 kv some of the beam is intercepted on the tungsten insert at the anode due to the size of the beam. Above 60 kv the beam size is smaller than the hole in the tungsten insert. This corresponds with the prediction of beam size plotted in Fig. 3.

The perveance of the 435-1C gun is shown in Fig. 10. The perveance of the gun measured $.125 \times 10^{-6}$ compared to 0.1×10^{-6} measured during the bell jar test on the gun.

The 435-1C gun focused with a much less magnetic field than required for the No. 9 and 435-1B guns used in tubes No. 1 and 2 as shown in Fig. 11. This improved focusing and larger beam size has allowed the operation of tube No. 3 at high average power levels than obtained previously with tube No. 1. In tube No. 1, which used the No. 9 gun, a great deal of difficulty was experienced in obtaining enough magnetic field for focusing due to the small beam size. The large magnetic field resulted in pole piece saturation and flux leakage back into the cathode region further complicating the focusing of the tube. A small beam size as in the case of tube No. 1, results in lower power and efficiency. The

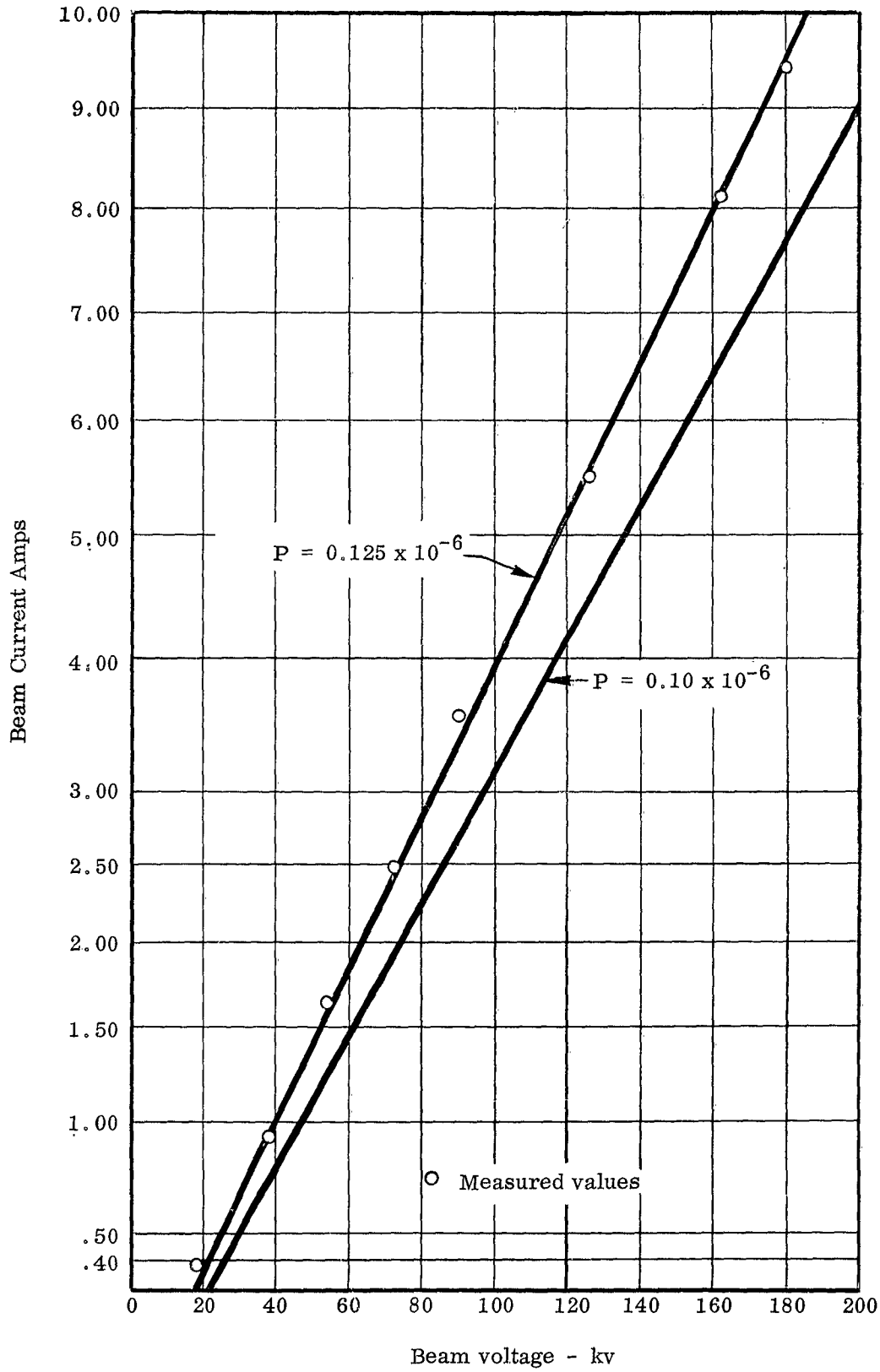

11763

Fig. 10 - Tube No. 3 beam current vs beam voltage plotted on 2/3 power graph paper. Perveance values of 0.1×10^{-6} and 0.125×10^{-6} are shown relative to the measured data.

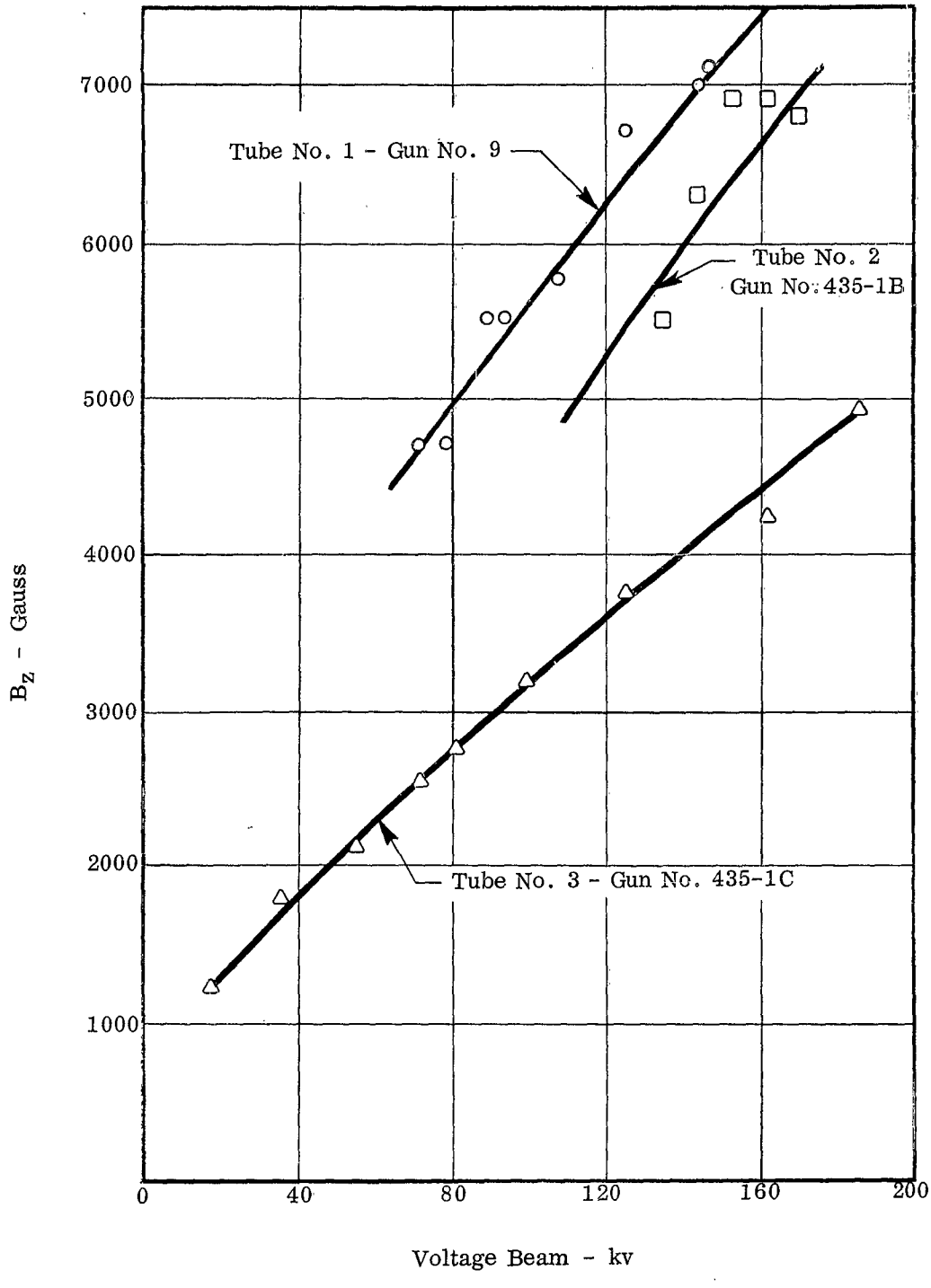

Fig. 11 - Magnetic field required to focus each of the three tubes built. The gun used in tube No. 3 requires the smallest magnetic field as shown by the curves.

beam size of the 435-1C gun is much nearer to the optimum size for the best efficiency, peak power and large average power which are the basic objectives of the program.

Measurement of Frequency

Testing of tube No. 3 has been conducted to date without the use of a frequency meter. The frequency meter used on previous tube tests was damaged. The waveguide was twisted off on one side of the cavity. This was repaired but the cavity did not respond when checked on the rf pulse of tube No. 3. Further efforts will be made to repair the frequency meter. Since the disk loaded waveguide circuit is the same as used on the previous tubes, the frequency vs beam voltage should be close to the values measured on tubes No. 1 and 2. Figure 12 shows this data for tubes one and two.

Average Power

Average power was measured using a Sierra Electronic Corporation Calorimeter, Model 190A. A new record, 300 watts of average power, was measured at a frequency near 100 Gc. A block diagram is shown in Fig. 13 of the calorimeter, the rf loads and water storage reservoir. The flow rate was maintained constant by using the water storage reservoir to maintain a constant 20 ft. head of water on the system. The water level in the reservoir is maintained constant by supplying excess water which is removed by the overflow. The water from the reservoir flows through one side of the thermopile then through the calibration coil to the rf load on the tube and back to the other side of the thermopile. Meter deflection corresponds to some $T_2 - T_2$ temperature difference at the thermopile as shown in Fig. 13.

Appendix II contains a discussion of the error in power measurement due to heat conduction from the waveguide load by the waveguide between the body of the tube and the rf load. It was found that more rf power is lost than calibration power. This means that the average power generated in the tube is greater than the measured value. The temperature of the waveguide between the tube body and the rf loads was measured at 70°C with 80 watts of average power.

Before higher average power measurements are made, the waveguide between the tube body and the rf loads will be water cooled in series with the rf loads. Table I lists some of the average power measurements made at various beam voltages. Later results have increased these values to over 300 watts.

Peak Power Measurements

The peak power of the tube was measured at 107 kw at 193 kv. This measurement was based on the average power and the duty cycle. The duty cycle was determined by the

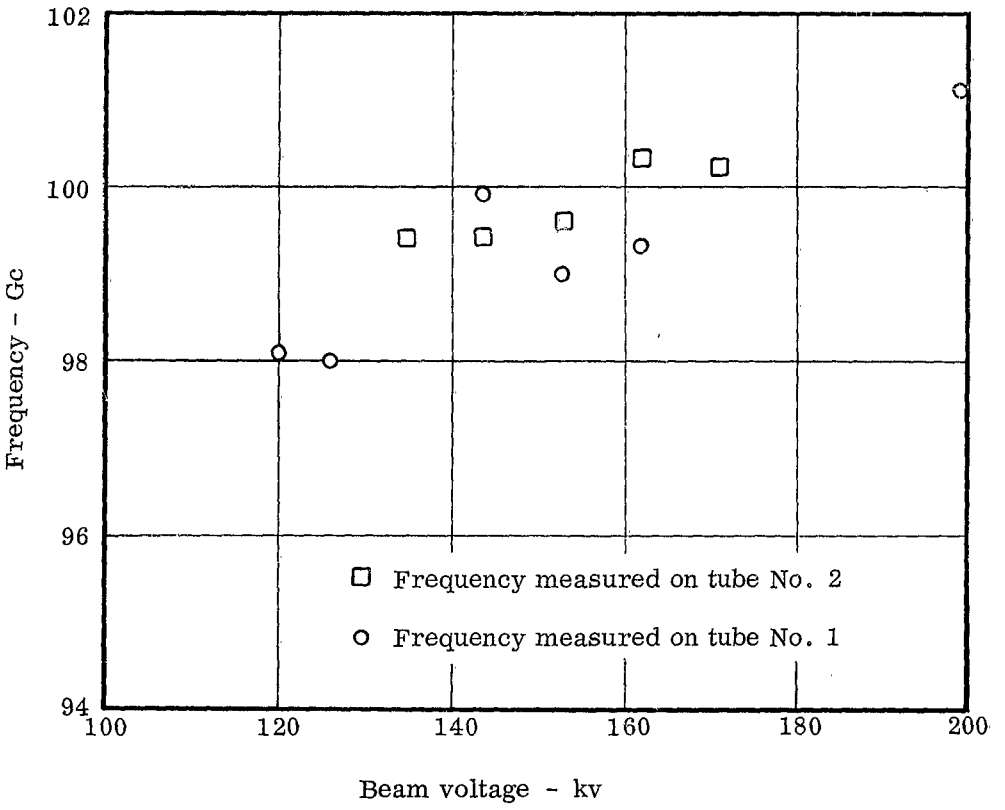

Fig. 12 - The frequency measured using a wavemeter vs beam voltage on tubes No. 1 and 2. The frequency of tube No. 3 should be close to these values shown above.

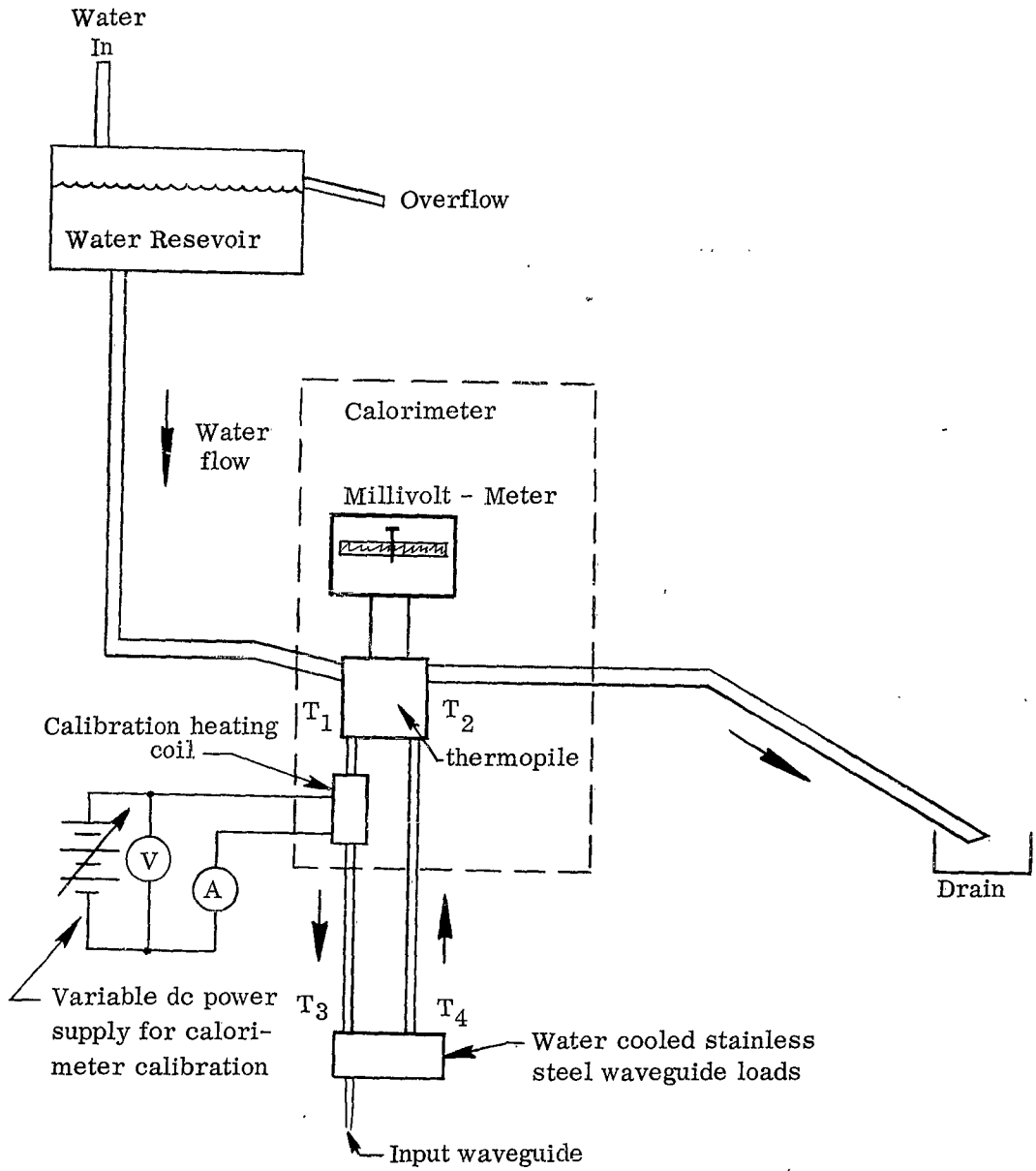

Fig. 13 - The average power of tube No. 3 was measured using the calorimeter arrangement shown above. Flow rate of water was 1/14 gallons per minute. The tube power is split equally between two output waveguides which are each terminated in water cooled stainless steel waveguide.

TABLE I

Voltage Beam	Average Power	RF Pulse-width	PRF	Peak Power
126 kv	30	3.16	200	47.5 kw
144	24	4.0	100	60.0 kw
162 kv	114	3.52	385	84.2 kw
162 kv	70	3.52	210	94.6 kw
175 kv	155	3.84	420	96 kw
175 kv	215	3.84	590	94 kw
193	75	4.20	167	107 kw

The peak power was calculated based on the average power measured using the calorimeter. The calorimeter was calibrated using a known source of dc power that had been calibrated against a secondary standard at the Watkins-Johnson Company. The duty cycles were determined by use of rf pusle shape photos and pulse interval measurement made on a Tektronix 531A oscilloscope. The rf pulse shapes are shown in the photographs in Figs. 20 to 24.

measurement of the pulse time interval on a Tektronix oscilloscope. The effective pulsewidth was calculated from the photos taken of the detected rf pulse as viewed on a Tektronix oscilloscope. A crystal was used as a detector and it was assumed that the crystal was a square-law detector. Figure 14 shows a detected rf pulse and its equivalent rectangular pulse. Both pulses have the same peak value and the same area in units of watt-sec. The equivalent pulsewidth is determined by numerical intergration to determine the area under the detected pulse. One can now determine the peak power as follows: The duty cycle equals pulsewidth x pulse repetition rate and peak power x duty cycle equals average power.

Table I lists the power levels, prf and pw resulting from tests on tube No. 3. A graph of peak power vs beam voltage is shown in Fig. 15. The curve is based on the average power measurement using the calorimeter at various duty cycles. Several points shown are measured using a crystal detector and a calibrated set of attenuators. The calibration of the crystal was based on past calibrations of similar crystals. It was necessary because a calorimeter was not available to calibrate the crystal. Results using the crystal did agree fairly well with the calorimeter results. This was probably a coincidence.

Pulse Shapes

The voltage current and rf pulse shape are shown in Figs. 16 to 25 at various beam voltages. Table II lists the parameter shown in the above figures. The rf pulse shapes do not have the holes that were present in the first two tubes. This indicates that the rf matches are better or there is less interaction with higher order modes, or both.

Beam Voltage

Beam voltage was measured on the primary side of the pulse transformer by use of a capacitive voltage divider and an oscilloscope. The voltage on the secondary of the pulse transformer is 18 times the primary voltage.

Higher Order Oscillation

There appears to be higher order mode oscillation at some voltages. This can be seen by the shape of the rf pulse at various voltage levels. The rf pulse as viewed at 193 kv has a reduced power level near maximum voltage. This reduction of power level may be due to oscillation. No check could be made to date on frequency due to lack of a frequency meter. Frequency measurement will be made when the wavemeter has been repaired.

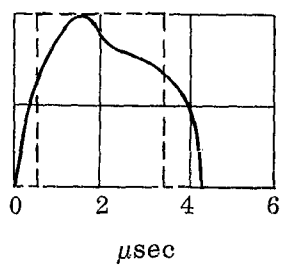

Fig. 14 - The solid line is the rf pulse viewed using a crystal detector and an oscilloscope. The rectangular pulse shown by the dash lines is an equivalent pulse with the same peak amplitude and area in terms of watt-seconds. The width of the equivalent pulse is determined by numerical intergration of the actual rf pulse. The above pulse occurred at a beam voltage of 126 kv and has an effective pulsewidth for calculating peak power of 3.16 micro-seconds.

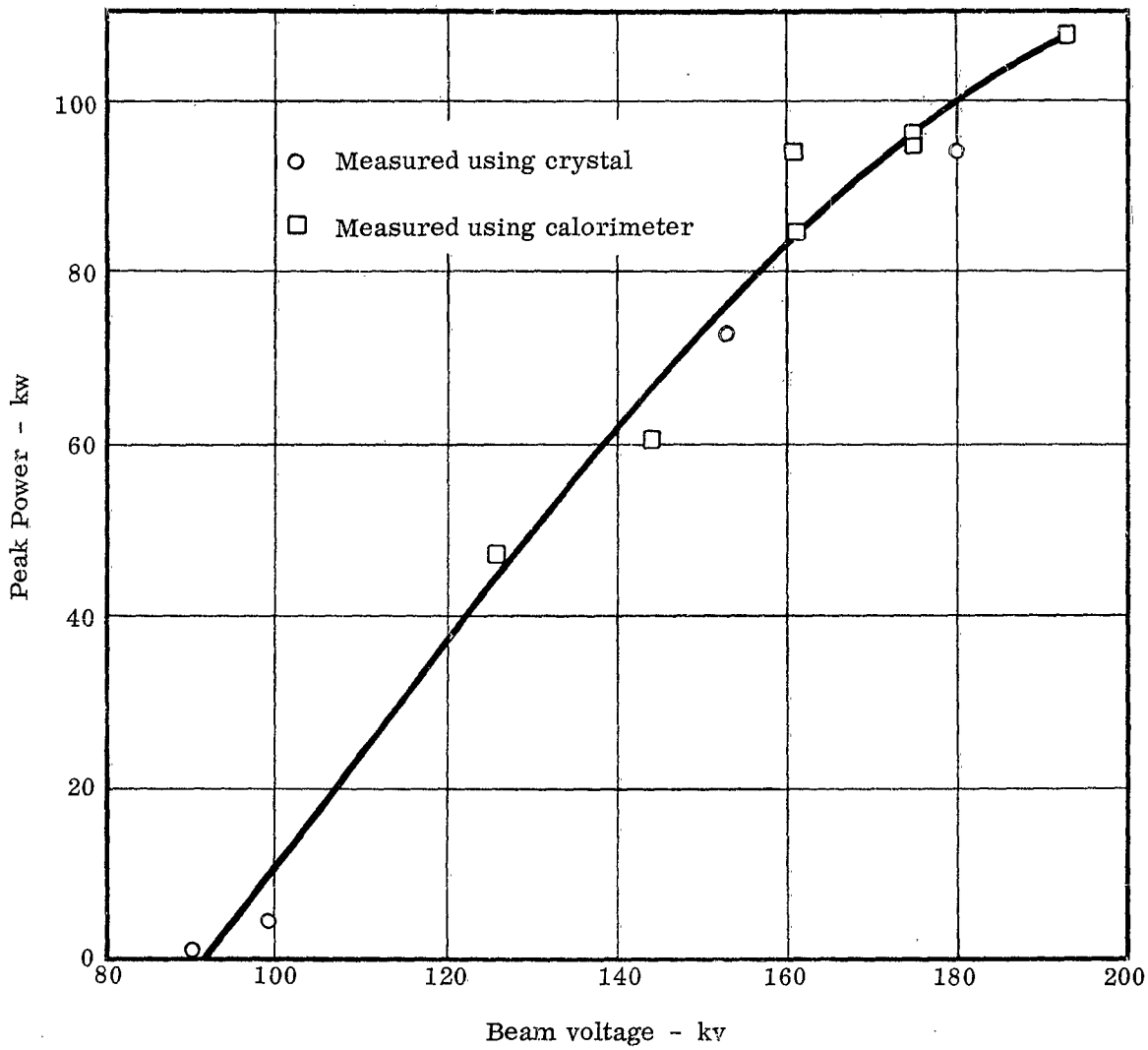

Fig. 15 - The graph shows the peak output power vs beam voltage. This data was measured using a crystal and attenuator and also by measurement of the average output power using a calorimeter. See Table I for the tabulated data using the calorimeter.

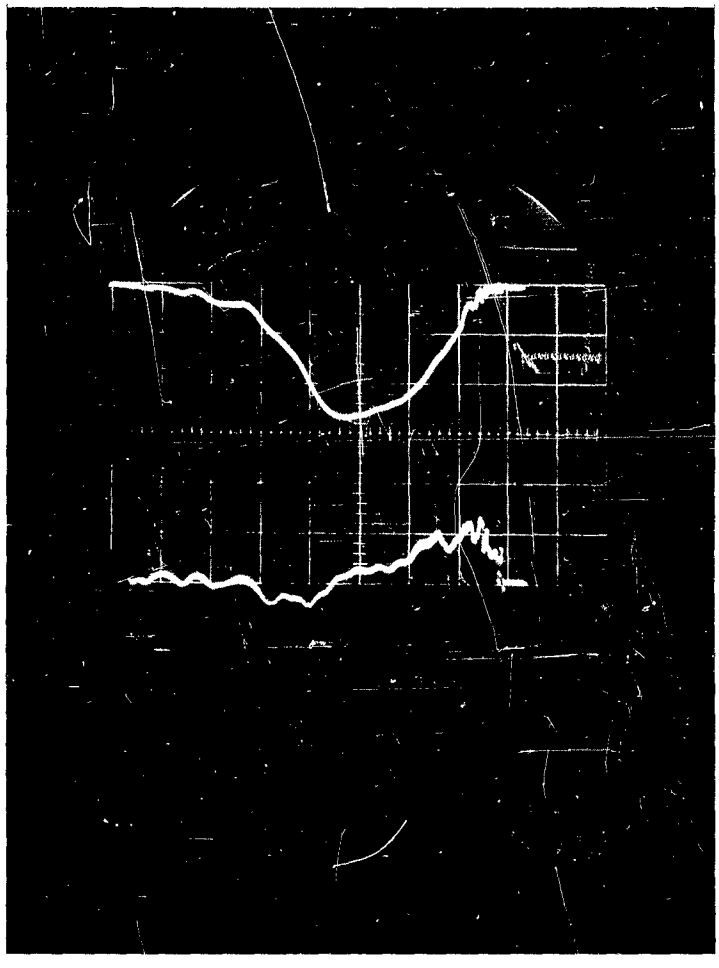

Fig. 16 - Collector and body current at 126 kv beam voltage. The top trace shows the collector current at 2 amps per cm. The bottom trace is the body current at 1 amp per cm. The time base is two microseconds per centimeter.

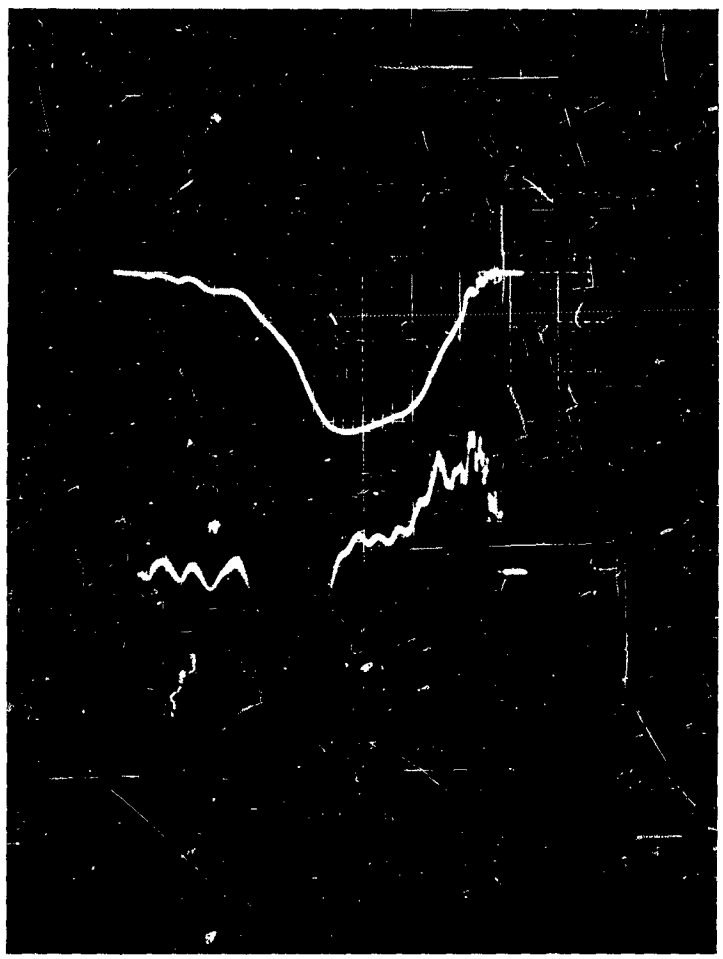

Fig. 17 - Collector and body current at 144 kv beam voltage. The top trace shows the collector current at 2 amps per cm. The bottom trace is the body current at 1 amp per cm. The time base is two microseconds per centimeter.

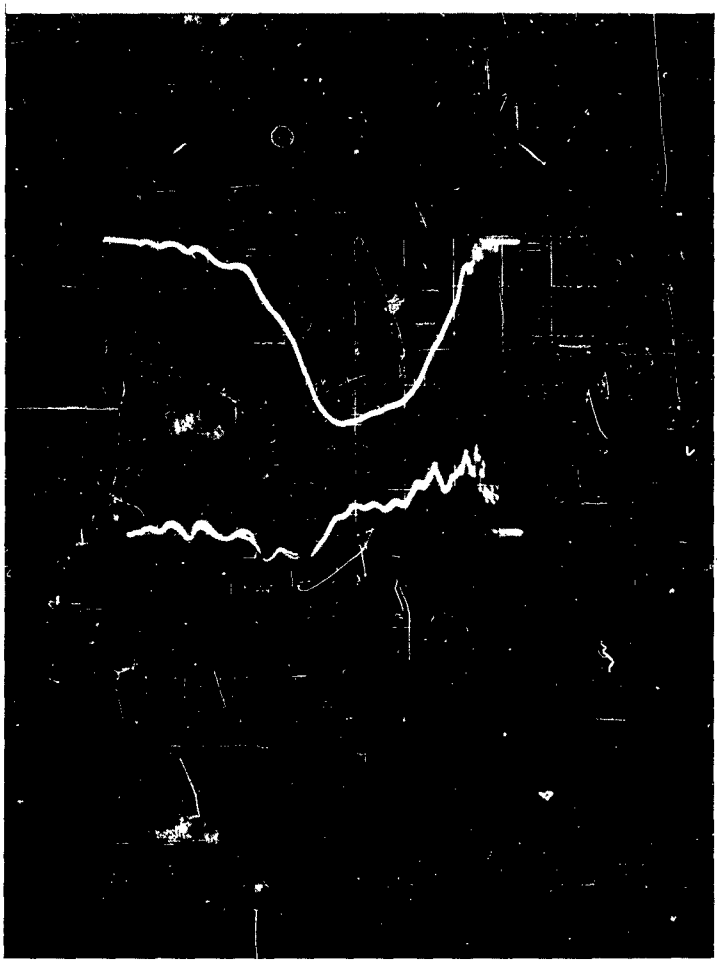

Fig. 18 - Collector and body current at 162 kv beam voltage. The top trace shows the collector current at 2 amps per cm. The bottom trace is the body current at 1 amp per cm. The time base is two microseconds per centimeter.

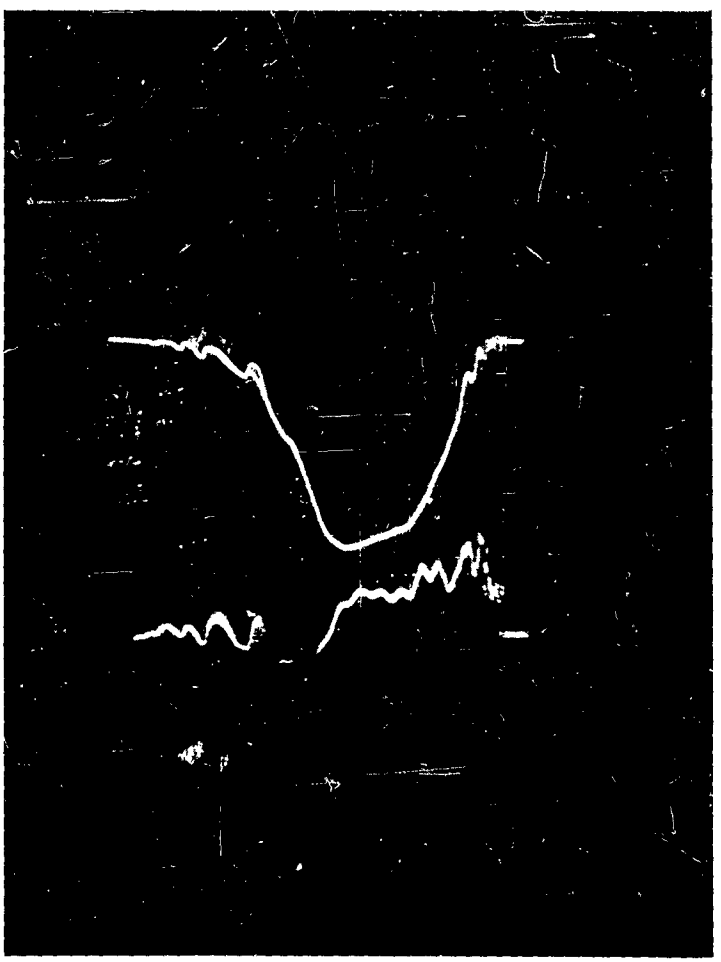

Fig. 19 - Collector and body current at 180 kv beam voltage. The top trace shows the collector current at 2 amps per cm. The bottom trace is the body current at 1 amp per cm. The time base is two microseconds per centimeter.

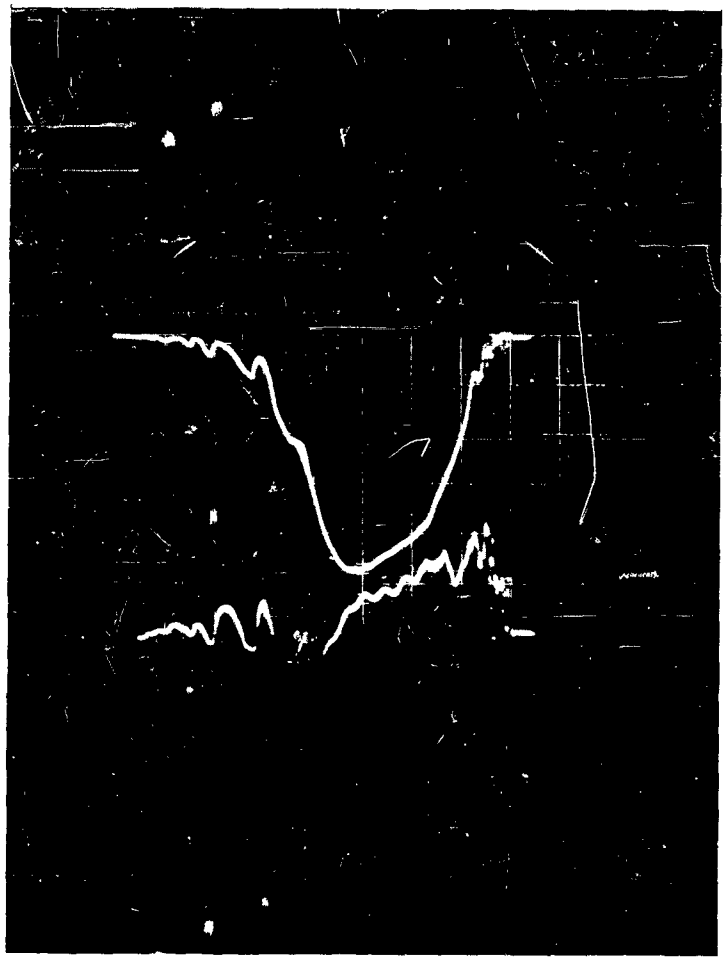

Fig. 20 - Collector and body current at 193 kv beam voltage. The top trace shows the collector current at 2 amps per cm. The bottom trace is the body current at 1 amp per cm. The time base is two microseconds per centimeter.

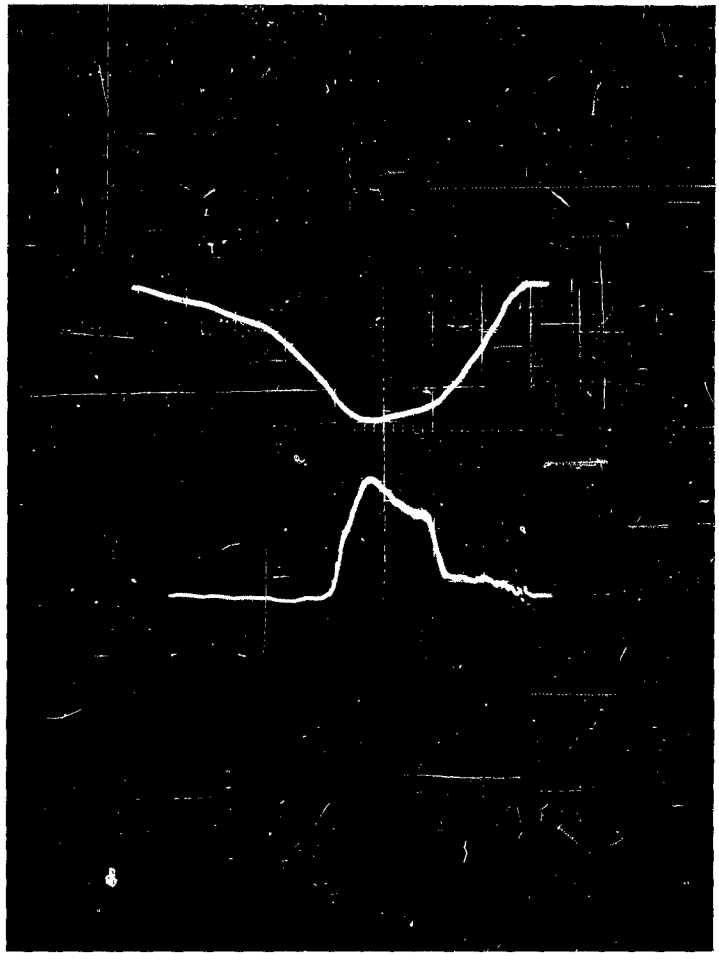

Fig. 21 - Cathode voltage pulse and detected rf pulse at 126 kv. Top trace is cathode voltage. Bottom trace is the detected rf pulse. There are no units of calibration vertically. The horizontal calibration is 2 microseconds per centimeter.

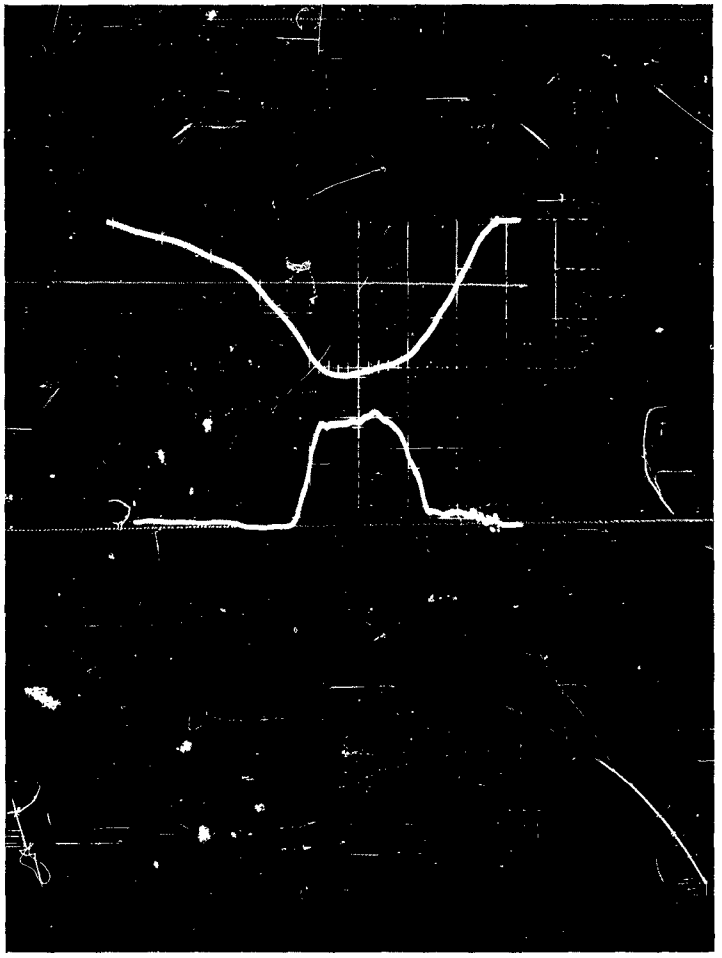

Fig. 22 - Cathode voltage pulse and detected rf pulse at 144 kv. Top trace is cathode voltage. Bottom trace is the detected rf pulse. There are no units of calibration vertically. The horizontal calibration is 2 microseconds per centimeter.

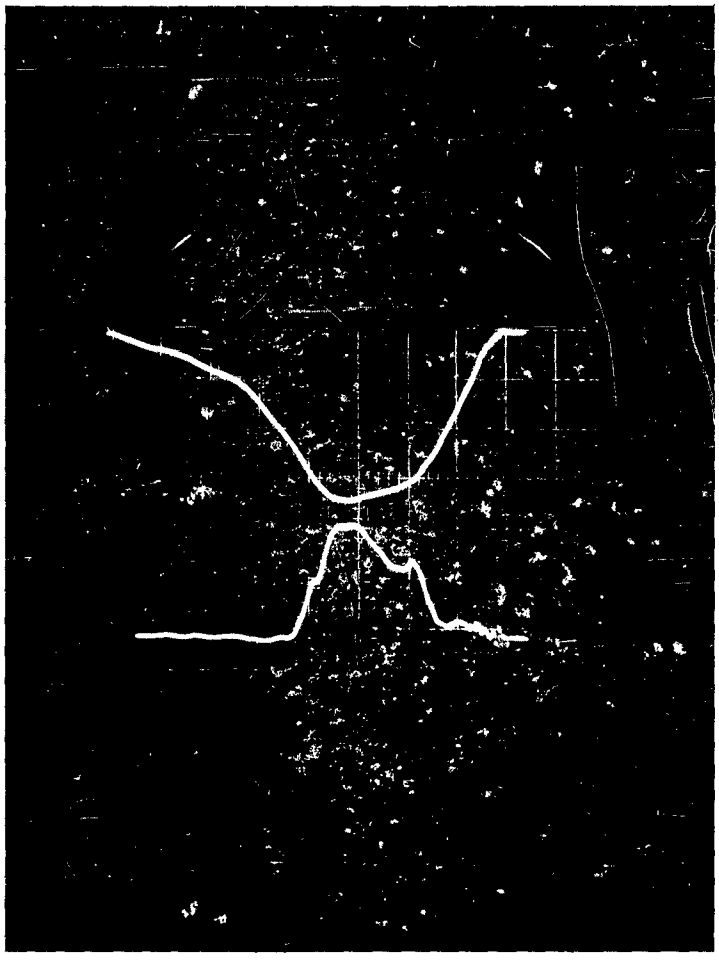

Fig. 23 - Cathode voltage pulse and detected rf pulse at 162 kv. Top trace is cathode voltage. Bottom trace is the detected rf pulse. There are no units of calibration vertically. The horizontal calibration is 2 microseconds per centimeter.

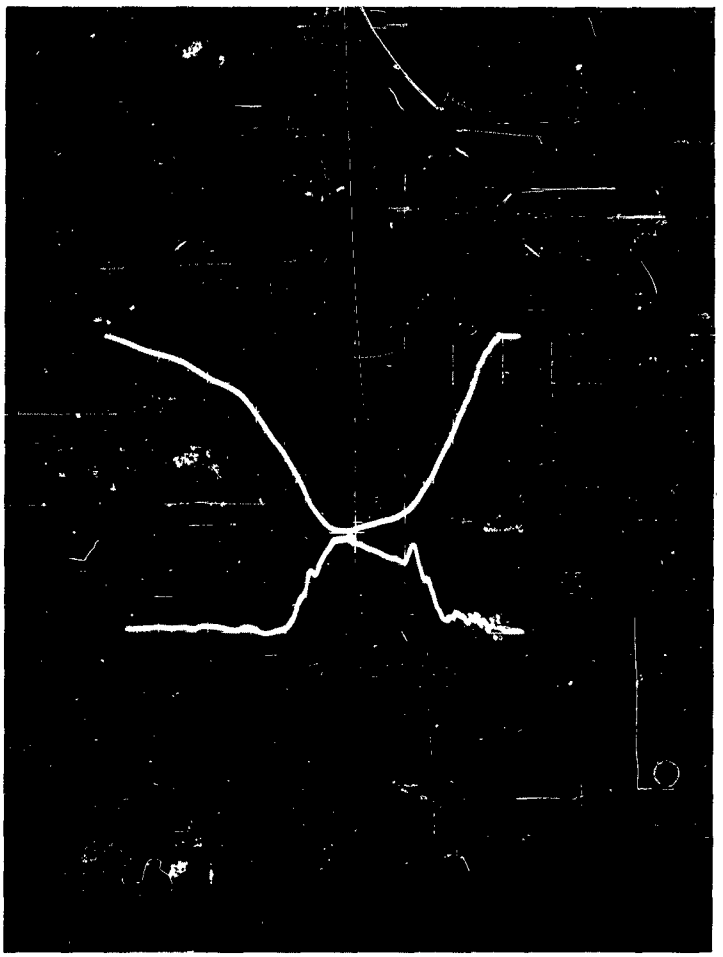

Fig. 24 - Cathode voltage pulse and detected rf pulse at 180 kv. Top trace is cathode voltage. Bottom trace is the detected rf pulse. There are no units of calibration vertically. The horizontal calibration is 2 microseconds per centimeter.

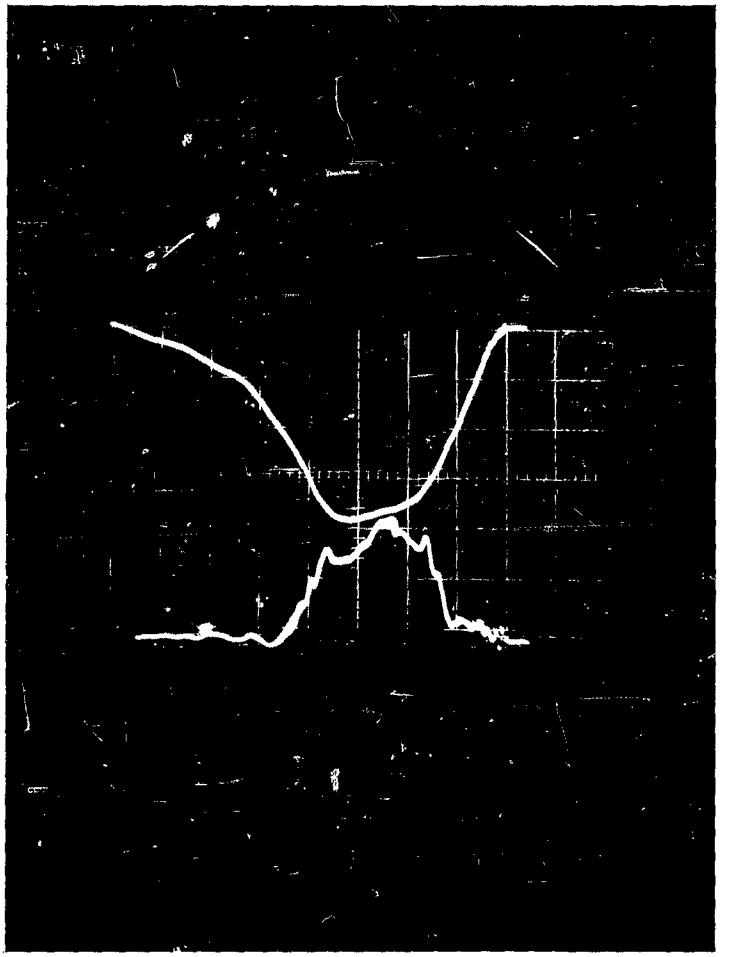

Fig. 25 - Cathode voltage pulse and detected rf pulse at 193 kv. Top trace is cathode voltage. Bottom trace is the detected rf pulse. Ther are no units of calibration vertically. The horizontal calibration is 2 microseconds per centimeter.

TABLE II

Figure No.	Beam Voltage	2 Amp/cm Collector Current	1 Amp/cm Body Current	Time Base
16	126 kv	Top-photo	Bottom - photo	$\frac{2\mu sec}{cm}$
17	144 kv	Top-photo	Bottom - photo	$\frac{2\mu sec}{cm}$
18	162 kv	Top-photo	Bottom - photo	$\frac{2\mu sec}{cm}$
19	180 kv	Top-photo	Bottom - photo	$\frac{2\mu sec}{cm}$
20	193 kv	Top-photo	Bottom - photo	$\frac{2\mu sec}{cm}$

Figure No.	Beam Voltage	Cathode Pulse Voltage Shape	RF Pulse Shape	Time Base
21	126 kv	Top - photo	Bottom - photo	$\frac{2\mu sec}{cm}$
22	144 kv	Top - photo	Bottom - photo	$\frac{2\mu sec}{cm}$
23	160 kv	Top - photo	Bottom - photo	$\frac{2\mu sec}{cm}$
24	180 kv	Top - photo	Bottom - photo	$\frac{2\mu sec}{cm}$
25	193 kv	Top - photo	Bottom - photo	$\frac{2\mu sec}{cm}$

Table II contains a list of the pulse shapes shown in Figs. 16 through 25. Figures 15 to 19 shows the body and collector current pulse shapes. Figures 20 to 25 shows the cathode voltages and detected rf pulse shapes.

REFERENCES

1. W. E. Danielson, J. L. Rosenfeld, J. A. Saloom "Analysis of Beam Formation with Electron Guns of the Pierce Type", BSTJ Vol. 35, pp. 375-420; March 1956.

2. G. B. Herrmann, "Optical Theory of Thermal Velocity Effects In Crylindrical Beams", Jour. Appl. Phys., Vol. 19, No. 2, pp. 127 to 136; February 1958.

3. Collins, "Microwave Magnetrons", Vol. 6, Radiation Laboratory Series, pp. 520 - 524.

APPENDIX I

Peak heating occurs during the current pulse due to beam interception on the circuit or anode. At 200 kv the power density in the beam is 281 megawatts per square centimeter. If this beam hits the circuit or anode, high surface temperature results which may melt the circuit.

To reduce the possibility of peak heating damage, a tungsten insert was used to collimate the beam as shown in Fig. 5. The following calculation shows tungsten to be 1.8 times poorer than copper in terms of temperature rise, but the melting point of tungsten is 3370°C compared with 1080°C for copper. For this reason tungsten was used as the insert material to reduce possible peak heating damage at the anode and in the rf circuit.

Calculations comparing tungsten and copper temperature rise due to peak heating. Calculations are based on Collins[3].

$$\Delta T = 2qa\sqrt{\frac{\tau}{\pi}}$$

$$q = \frac{1}{K}\ 0.239\ D$$

$$a = \sqrt{\frac{K}{C\rho}}$$

K = Thermal conductivity in $\frac{\text{cal}}{\text{sec - cm }^{\circ}\text{C}}$

D = Power density in watts/cm^2

τ = Pulsewidth in sec

ρ = Density in gram/cm^3 C = Specific heat in cal/gram/°C

For copper:

K = 0.9
C = .126
ρ = 8.9

For tungsten:

K = 0.4
C = .039
ρ = 19.6

ΔT is porportional to $\frac{1}{\sqrt{KC\rho}}$ for a constant power density and pulsewidth

$$\frac{\Delta T\ (\text{tungsten})}{\Delta T\ (\text{copper})} = \frac{\sqrt{KC\rho}\ (\text{copper})}{\sqrt{KC\rho}\ (\text{tungsten})} = 1.8$$

APPENDIX II

A Discussion and Some Calculations On Calorimeter Calibration

In Fig. 13 a given temperature difference between $T_2 - T_1$ produces a certain deflection on the calorimeter meter. This deflection can be produced either by supplying power to heat the water at the calibration heating coil in the calorimeter, or by heat generated by the dissipation of rf power in the rf loads.

During the measurement of average power, the meter reads a value corresponding to some $T_2 - T_1$. The tube is turned off and the calibrating power turned on to produce the same deflection on the meter thus the same $T_2 - T_1$ temperature difference. The power used in the calibrating coil should correspond to the average power dissipated in the rf loads of the tube. This is true if none of the rf or calibration power is lost by radiation, convection or conduction. At low temperature radiation loss is extremely small. The rf load should lose little power by air convection, but heat transfer by conduction between the tube body and rf loads may introduce an error between the calibration power level and the correct rf power. The following calculation is made to determine if more power is lost during calibration or if during the measurement of rf. If more power is lost during the measurement of rf power then rf average power is greater than the calibration value.

The power lost to the tube body by conduction is lost through the waveguide between the tube body and the rf load. If more power is conducted back to the tube body during power measurement than during calibration the temperature of the waveguide between the body and the loads must be larger during the rf power measurement than during the calibration. This is the case. Power is dissipated in the waveguide during tube operation raising the temperature on the guide above the water temperature in the rf loads. At 80 watts of average power, the temperature of the waveguide was measured at 70°C one inch below the rf load on the waveguide. Based on this measurement of guide temperature, the following calculations can be made to show that the rf power is greater than the calibration power over a range of power levels.

Formula used in the following calculation:

(1) $P = 264\, Qw\ \Delta T$ (heat transfer by water)

P = Power in watts

Qw = Watts flow in gallon per minute

ΔT = Outlet and inlet water, temperature difference in degrees centigrade, respectively

(2) $$P = \frac{AK}{Z} \Delta T$$ (heat transfer by conduction)

P = Power in watts

A = Cross-sectional area

K = Specific heat conductivity

Z = Length

ΔT = Temperature difference ^{o}C

P_c = Power used to calibrate

P_{rf} = Power output of the tube

P_{lc} = Power lost by conduction during calibration

P_{lrf} = Power lost by conduction during rf power measurement

$$P_c - P_{lc} = P_{rf} - P_{lrf}$$

$$\frac{P_{rf}}{P_c} = \frac{P_c - P_{lc} + P_{lrf}}{P_c}$$

$$P_{lc} = \frac{AK}{Z} (T_1 - T_B)$$

T_B = Temperature of tube body maintained at $20^{o}C$ by cooling water during both calibration and rf power measurements

T_o = Water inlet temperature to calorimeter = $20^{o}C$

T_1 = Water temperature in rf loads during calibration

$$T_1 - T_o = \frac{P_c}{264\ Qw}$$

Qw = Water flow rate of calorimeter

$$P_{1c} = \frac{AK}{Z} \quad \frac{P_c}{264\ Qw}$$

Z is larger than length to the point where temperature was measured at 70°C at 80 watt power.

$$P_{1rf} \quad \frac{AK}{Z} \ (70^{o} - 20) \ = \ \frac{AK}{Z} \ 50^{o}$$

$$\frac{P_{rf}}{P_c} \geq 1 + \frac{AK}{Z} \left(\frac{50}{P_c} - \frac{1}{264\ Qw} \right)$$

$$\frac{P_{rf}}{P_c} \geq 1 \text{ if } \frac{50}{P_c} \geq \frac{1}{264\ Qw}$$

$$P_c < (50)(264)\ Qw$$

Qw was measured at 1/14 gallon per minute

$$P_c < 942 \text{ watts}$$

$$\frac{P_{rf}}{P_c} \geq 1 \text{ for power levels above 80 watts and less than 942 watts}$$

The correct rf average power is greater than the calibrating power over a range of powers from 80 watts to 942 watts, based on the measurement of the waveguide temperature between the body and the rf load. It could be shown that for a much larger range of power levels

$$\frac{P_{rf}}{P_c} \geq 1$$

by measurement of waveguide temperatures at other power levels. On the basis of the above calculation and the measurement of waveguide temperature, the new record of 215 watts average power at 100 Gc is at least as large as 215 watts.

DISTRIBUTION LIST

AF 33(616)-8369

Destination	Copies
Aeronautical Systems Division Air Force Systems Command United States Air Force Wright-Patterson Air Force Base Dayton, Ohio Atten: ASRNET-1, Contract AF 33(616)-8359, Item No. 1	4 and 1 Reproducible
ASTIA (TISIA) Arlington Hall Station Arlington 12, Virginia	20
Advisory Group on Electron Devices 346 Broadway, 8th Floor New York 13, New York Attention: Mr. H. N. Serig	4
Air Force Cambridge Research Laboratories L. G. Hanscom Field Bedford, Mass. Attention: Mr. R. W. Wagner	1
Electronic Systems Division L. G. Hanscom Field Bedford, Mass. Attention: ESRDE, Major J. W. Van Horn	1
Rome Air Development Center Griffiss Air Force Base New York Attention: RALTP, Mr. H. Chiosa	1
Commanding Officer U. S. Naval Ordnance Laboratory Corona, California Attention: Miss Virginia L. Parker	1

Distribution List (continued)

	Copies
Chief, Bureau of Ships Code 691A4 Department of the Navy Washington 25, D. C. Attention: Mr. H. J. Riegger	1
Chief, Bureau of Ships Department of the Navy Washington 25, D. C. Attention: Mr. Charles Walker	1
Commanding Officer USAERDL SIGRA/SL-PRM Fort Monmouth, New Jersey Attention: Mr. Harold J. Hersh	1
Commanding Officer USAERDL Microwave Tubes Branch Fort Monmouth, New Jersey Attention: Mr. Irving Reingold	1
Commanding Officer Diamond Ordnance Fuze Laboratories Microwave Tube Branch Washington 25, D. C.	1
G. E. Traveling Wave Tube Product Section 601 California Avenue Palo Alto, California Attention: Technical Library	1
Hughes Research Laboratories Malibu, California Attention: Dr. M. Currie	1
Litton Industries, Inc. 960 Industrial Road San Carlos, California Attention: Dr. J. Hull	1

Distribution List (continued)

	Copies
Raytheon Corporation Waltham, Massachusetts Attention: Dr. P. Derby	1
Bendix Corporation Research Laboratories North Western Hwy and 10 1/2 Mile Rd. Southfield, Michigan Attention: Mr. A. G. Peifer	1
Radio Corporation of America 415 South Fifth Street Harrison, New Jersey Attention: Mr. H. K. Jenny 55-2	1
Sperry Gyroscope Company Great Neck, New York Attention: Dr. L. W. Holmboe	1
Aerospace Corporation 2400 E. El Segundo Blvd. El Segundo, California Attention: Mr. B. J. DuWaldt	1
Director U. S. Naval Research Laboratory Washington 25, D.C. Attention: Code 5240	1
Director U. S. Naval Research Laboratory Washington 25, D. C. Attention: Code 5244, Mr. H. D. Arnett	1
Scientific and Technical Information Facility P. O. Box 5700 Bethesda, Maryland Attention: NASA Representative (S-AK/DL)	1